Impact of Thermal and Environmental Conditions on the Kinect Sensor

David Fiedler and Heinrich Müller

Department of Computer Science VII, Technische Universität Dortmund,
Otto-Hahn-Straße 16, 44227 Dortmund, Germany
{fiedler,mueller}@ls7.cs.uni-dortmund.de

Abstract. Several approaches to calibration of the Kinect as a range sensor have been presented in the past. Those approaches do not take into account a possible influence of thermal and environmental conditions. This paper shows that variations of the temperature and air draft have a notable influence on Kinect's images and range measurements. Based on these findings, practical rules are stated to reduce calibration and measurement errors caused by thermal conditions.

Keywords: Kinect Sensor, Calibration, Thermal Influence

1 Introduction

Many applications utilize the Kinect [12], originally an input device of the Microsoft Xbox video game console, as a range sensor, e.g. [2, 4]. Several comparisons of accuracy between Kinect's depth data and other range systems, like laser range scanners [3], Time-of-Flight cameras [1] or PMD cameras [5], have been evaluated. All these works perform geometric (intrinsic and distortion parameters) and depth (range) calibration to increase accuracy, but do not consider thermal and environmental conditions, neither during the calibration phase, nor during the measurement or evaluation phase.

The contribution of this paper experimentally demonstrates that variations of temperature as well as air draft significantly affect the range measurement of the Kinect. Air draft can cause changes of the depth values up to 21 mm at a total distance of 1.5 m, and temperature variations cause changes up to 1.88 mm per 1°C difference. The necessary warm-up time to rule out temperature-induced errors is up to 60 minutes. Depending on its thermal state, Kinect's RGB camera shows a shift of projected objects up to 6.7 pixels measured with an optical flow approach. This observation is also important for range calibration since many approaches involve the RGB camera. The findings are transferred into rules which help to reduce measurement errors.

The following section gives a brief survey of related work. Section 3 is devoted to the influence of different thermal states to the optical lens system of both internal cameras (RGB and IR). Section 4 presents several experiments based on different approaches of distance measurements and different environmental conditions. Conclusions are given in section 5.

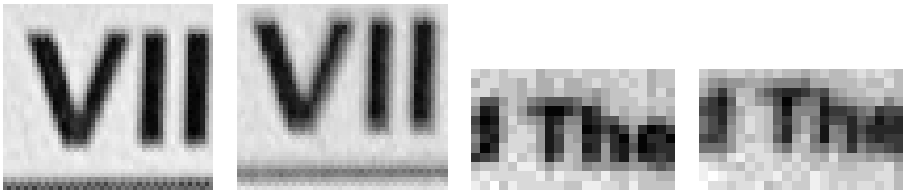

(a) RGB cold state (b) RGB warm state (c) IR cold state (d) IR warm state

Fig. 1. Close-up views of small regions that were cropped out from the image of the texture-rich poster shown in Fig. 2(a).

2 Related Work

The influence of temperature in the context of imaging and range sensors has been studied in the past. In the field of aerial mapping, lenses were put into large refrigerators to simulate the temperature in high altitudes and to calibrate them under these conditions [14]. The dependency of range values on temperature for the Swiss Ranger SR-2 Time-of-Flight camera was analyzed in [6]. The effect of temperature variations on intrinsic parameters of SLR-cameras has been studied in [15]. However, the influence of temperature and other environmental conditions has not been investigated for the Kinect sensor so far.

3 Thermal Influence on Kinect's Optical Camera Systems

To determine the thermal influence on the optical systems of both internal cameras, we tested the Kinect at two different thermal conditions (heat states). In one case (called cold state) the Kinect was cooled down by an externally mounted fan (cf. Fig. 3(c)) which slowly streams air through the Kinect's body and cools down its internal components to the environmental temperature of 27.6°C. In the other case (called warm state) the fan was deactivated and the Kinect was warmed up just by processing the color and depth image-stream for 45 minutes. The fan was always accelerated smoothly to prevent motion of the Kinect.

Image Based Comparison. A texture-rich poster (cf. Fig. 2(a)) was captured by both cameras at both heat states. Comparing pictures taken in different heat states, two changes could be observed for the warm state: the pictures were more blurred and the poster appeared slightly magnified. Although the cropped areas of the close-up views in Fig. 1 had the same size and pixel-position for both heat states, a shift of the letters and a loss of sharpness can be noticed.

Comparison based on Dense Optical Flow. A dense optical flow approach [7] has been applied to image pairs of the poster taken in both heat states. For visualization, the color-code proposed in [8] was used (cf. Fig. 2(b)). The magnitude of the optical flow was small near the image center and large at its margins (cf. Fig. 2(c) and 2(d)). The maximal flow was 6.7 pixels for the RGB and 1.8 pixels (note the smaller IR image resolution) for the IR camera.

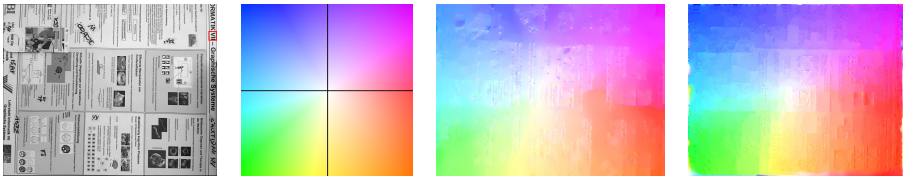

(a) Poster (b) Color code (c) IR opt. flow (d) RGB opt. flow

Optical Flow	Image resolution	Maximal flow	Horizontal Range	Vertical Range
RGB	1280x1024	6.7338	-6.440 .. 4.897	-5.044 .. 3.678
IR	640x480	1.7853	-1.666 .. 1.581	-1.461 .. 1.115

Fig. 2. Texture-rich poster (a) observed by both cameras in both heat states. In the color coding scheme (b), hue indicates direction and saturation indicates magnitude. White color indicates no movement, strong colors indicate large movements. The results of the dense optical flow from the cold to the warm state are shown in (c) for the IR and in (d) for the RGB camera. The table summarizes quantitative details.

Parameter	f_x	f_y	c_x	c_y	p_1	p_2	p_3	q_1	q_2	Error
RGB										
Cold	1041.60	1043.29	656.70	520.56	0.18314	-0.51989	0.45196	0.00012	0.00122	0.07146
Warm	1046.25	1048.14	656.87	523.67	0.19178	-0.55455	0.50113	0.00069	0.00144	0.06770
Difference	4.65	4.85	0.17	3.10	0.00864	-0.03466	0.04917	0.00057	0.00022	-0.00376
IR										
Cold	586.02	586.78	321.27	239.21	-0.10137	0.46481	-0.6413	-0.00112	-0.00009	0.02704
Warm	587.14	588.04	322.70	238.15	-0.11278	0.5179	-0.71455	-0.00213	-0.00013	0.02438
Difference	1.12	1.25	1.43	-1.06	-0.01141	0.05309	-0.07325	-0.00101	-0.00004	-0.00266

Table 1. Comparison of calibration parameters of the RGB camera (upper table) and the IR camera (lower table) for the cold and warm state.

Regarding the color distribution and the magnitude, the observations can be interpreted as a zoom-in effect.

Comparison Based on Calibration Parameters. If the previous observations are caused by a thermally dependent deformation or shift of the optical lens system, we expect a change in the parameters of the camera model and the lens distortion model. A calibration plane with checker pattern was placed in front of the Kinect at 23 different orientations and captured simultaneously by both cameras. Repeating this for both heat states, we got two sets of images for each camera. The IR projector was blocked to prevent detection errors of checkerboard corners by the structured light. Each set of images was used to determine the parameters using the MATLAB camera calibration toolbox [11]. Table 1 shows the results. For both cameras the focal length increases in the warm state, which is consistent with the zoom-in effect revealed by the optical flow approach. No significant changes of the back-projection error [10] could be observed. Thus we can assume that the employed camera model fits well for both heat states. Note that both cameras are sensitive to thermal changes, especially the RGB camera. This is important for calibration approaches that involve the RGB camera within their range calibration like in [1]. We conclude the following rule: *Camera calibration and subsequent measurements should be performed at the same thermal conditions.*

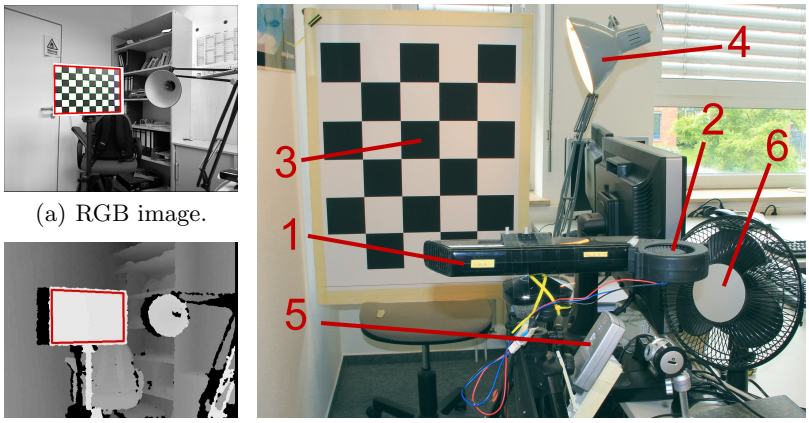

(a) RGB image.

(b) Depth image.

(c) Experimental setup in a static scene.

Fig. 3. The region of interest (red box) within the RGB camera image (converted to grayscale) and the depth image are shown in (a) and (b). The experimental setup consists of the following items: Kinect (1), mounted fan (2), large planar checkerboard (3), fluorescent lamp (4), thermometer (5), table fan (6).

4 Thermal Influence on Range Measurement

The experimental evaluation of thermal influences on range measurements used mean distances to a checkerboard of size 0.75×1.0 m at a distance of 1.5 m placed in front of a Kinect mounted with a fan, cf. Fig. 3(c). The mean distances were determined in two ways. Both Kinect cameras were calibrated in advance, using sets of images generated in the cold state, to obtain intrinsic as well as radial and tangential distortion parameters. Furthermore, a stereo calibration of the cameras was performed simultaneously as described in [9].

Mean Distance Calculation based on the Model Plane. The mean distance $\mathcal{D}^{\mathcal{MP}}$ from the RGB camera to the checkerboard is determined as follows:

- Detect the checkerboard within the current image (see the red box in Fig. 3(a) where the region of interest (ROI_{RGB}) is marked).
- Construct a 3D-model of the checkerboard (denoted as model plane).
- Calculate the 3D rotation matrix $\mathbf{R}_m$ and the translation vector $\mathbf{t}_m$ of the model plane relatively to the camera, so that the back-projection error is minimized (see [10] for details).
- Define 3D-rays from the camera center $\mathbf{c}_0$ to every pixel within the ROI_{RGB}.
- Finally, calculate the mean of all single distances between $\mathbf{c}_0$ and the intersection point of each 3D-ray with the model plane.

Mean Distance Calculation based on Depth. The checker pattern was not visible in the depth image. Thus the checkerboard model, whose position in the coordinate frame of the RGB camera was given by $\mathbf{R}_m$ and $\mathbf{t}_m$, was transformed to the coordinate frame of the IR camera using the rotation matrix

$\mathbf{R}_s$ and the translation vector $\mathbf{t}_s$ between the frames of both cameras available from the stereo calibration. Then the checkerboard model was projected onto the image plane of the IR camera to get the ROI_{IR}. According to [1], there is a pure shift between the IR and the depth image of three pixels in x- and y- direction. Thus, we just shifted the ROI_{IR} to get the ROI_D within the depth image (cf. Fig. 3(b)). For each pixel within the ROI_D we calculated the corresponding 3D-point in space using the OpenNI framework [13]. Finally, the mean of all magnitudes of these 3D-points is the desired mean distance $\mathcal{D}^{\mathcal{D}}$ based on depth data.

4.1 Tracking Distances after Power-On

The Kinect was disconnected for three hours to cool it down to the room temperature of 27.7°C before starting the tracking of both distances during the warm-up phase. Fig. 4(a) shows the plots within 135 minutes. A decrease of -6.97 mm was observed for $\mathcal{D}^{\mathcal{MP}}$. 90% thereof took 60 minutes of warm-up time. We suppose that this change is a direct consequence of the zoom-in effect (cf. Sec. 3): the checkerboard appears to have moved towards the camera and thus the measurement of $\mathcal{D}^{\mathcal{MP}}$ outputs a smaller checkerboard distance, although the scene was not changed. The measured change in $\mathcal{D}^{\mathcal{D}}$ was an increase of 19.49 mm. 90% thereof occurred within 41 minutes. Since the effect of lens deformation of the IR camera was smaller compared to the RGB camera (cf. Sec. 3), the change in $\mathcal{D}^{\mathcal{D}}$ is not explainable only by this effect. However, for typical indoor scenarios we can state the rule: *A warm-up time of up to 60 minutes is necessary to reach stable measurement conditions.*

4.2 Distance Changes between Thermal States

The following experiment was performed at a constant room temperature of 27.5°C. We used the mounted fan and alternated between phases with and without fan cooling to change the heat state and tracked again the distances (cf. Fig. 5). The experiment was repeated three times. The cool down was completed within 10 and 18 minutes for $\mathcal{D}^{\mathcal{D}}$ and $\mathcal{D}^{\mathcal{MP}}$, respectively. The longest warm-up period was finished after 61 minutes regarding $\mathcal{D}^{\mathcal{MP}}$. This is comparable to the results in Sec. 4.1. Regarding $\mathcal{D}^{\mathcal{D}}$, the warm-up took 33 minutes. The ventilation had a strong impact on the measurements, although the room temperature was stable. $\mathcal{D}^{\mathcal{MP}}$ increased by 5.67 mm while $\mathcal{D}^{\mathcal{D}}$ decreased by -22.76 mm during fan cooling.

The arrows in Fig. 5 mark the points in time where erratic changes between 2 and 4 mm occurred in the plot of $\mathcal{D}^{\mathcal{D}}$. At the same time a rapid and global change in the values of the corresponding depth image could be noticed. Erratic changes occurred in situations of rapid temperature variations of Kinect's internal components. In a decreasing phase they performed an upward correction and vice versa.

4.3 Distance Changes caused by Air Draft

During this experiment the room temperature was constantly 27.5°C. To simulate air draft, we used a standard table fan (cf. Fig. 3(c)). It was blowing sideways at the Kinect in the warm state at a distance of 30 cm for only 10 seconds. The changes in $\mathcal{D}^{\mathcal{MP}}$ were insignificant. However, regarding $\mathcal{D}^{\mathcal{D}}$, even this very short period of time caused a change of -3.22, -3.14, and -3.18 mm for three repetitions of this experiment. The necessary warm-up time to reach the initial distance values took between 5 and 6 minutes in each repetition. Due to the described high sensitivity, the following rule can be established: *Try to avoid air draft while using the Kinect in the warm state.*

4.4 Tracking Temperature and Distance Changes

We demonstrate Kinect's sensitivity to naturally occurring temperature changes in an everyday scenario. The investigations took place in a room of size 5×3×3 m with a digital thermometer mounted 10 cm beneath the Kinect (cf. Fig 3(c)). The door and windows were closed before the experiment started. At the beginning, the room temperature was 26.2°C and we opened a window. Air draft was prevented by blinding the window and keeping the door closed. Weather changes (mix of sun and rain) caused indoor temperature variations. At minute 497 the window was closed and the room temperature increased. In Fig. 4(b), a negative correlation between temperature (green) and $\mathcal{D}^{\mathcal{MP}}$ (blue) can be observed. This conforms to the zoom-in effect (cf. Sec. 3). In contrast to that, a positive correlation between temperature and $\mathcal{D}^{\mathcal{D}}$ (red) can be noticed. The maximal temperature difference was 3.4°C. This caused a maximal change of -1.9 mm in $\mathcal{D}^{\mathcal{MP}}$ and 6.39 mm in $\mathcal{D}^{\mathcal{D}}$, what means a change of -0.56 and 1.88 mm per 1°C. The latter compares well with an increase by 8 mm per 1°C as reported for the SR2 time-of-flight camera [6]. The table in Fig. 4(b) shows quantitative details.

4.5 Distance Changes after Stand-By and USB Disconnection

In these experiments the environmental conditions were constant (constant temperature, no air draft, no fan, closed door and windows). Before starting, the Kinect was on-line (streaming depth and RGB images) to warm up. The amount of changes caused by two types of working interruptions within a long-term use of the Kinect will be examined in the following. This investigation has practical relevance because such interruptions are typical while working with the Kinect or developing software with interleaved testing phases.

Type 1: Disconnection from USB or Power. Some pretests revealed that the power supply as well as the USB disconnection produced the same results. This is traceable since the Kinect stopped power consumption if USB was disconnected. Thus, there was no heating of internal components in both cases. The Kinect was disconnected for 2, 5, and 10 minutes resulting in a change of -6.12, -10.38, and -14.66 mm in $\mathcal{D}^{\mathcal{D}}$. Regarding $\mathcal{D}^{\mathcal{MP}}$, 0.32, 1.21, and 2.36 mm

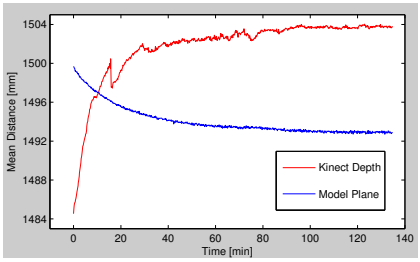

(a) Evaluation after power-on.

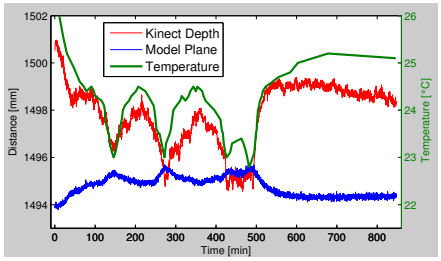

(b) Influence of temperature variations.

Power-On	Start	End	Diff.	90%
Kinect Depth[mm]	1484.54	1504.03	19.49	41.0 min
Model Plane[mm]	1499.68	1492.71	-6.97	62.9 min

Temp. influence	Min	Max	Diff.	mm/°C
Temperature [°C]	22.8	26.2	3.40	-
Kinect Depth[mm]	1494.57	1500.96	6.39	1.88
Model Plane[mm]	1493.79	1495.69	1.90	-0.56

Fig. 4. Plots of $\mathcal{D}^{\mathcal{D}}$ (red) and $\mathcal{D}^{\mathcal{MP}}$ (blue) as well as the environmental temperature (green) over time. The erratic change in (a) at minute 15.9 will be discussed in Sec. 4.3. Each table beneath the plots summarizes quantitative details.

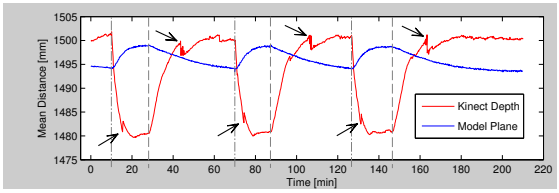

Fig. 5. Track of distances in alternating phases with and without cooling using a mounted fan. Dot-dashed lines mark time points of fan activation, dashed lines indicate deactivations. Arrows mark time points where erratic distance changes occurred.

were observed. These small values are valid since $\mathcal{D}^{\mathcal{D}}$ and $\mathcal{D}^{\mathcal{MP}}$ base on mean distances with a low noise level measured below $\sigma_{\mathcal{D}^{\mathcal{D}}} = 0.35$ and $\sigma_{\mathcal{D}^{\mathcal{MP}}} = 0.12$ mm in all stable heat states. After 10 minutes of disconnection, 18 and 57 minutes were needed to reach stable values again for $\mathcal{D}^{\mathcal{D}}$ and $\mathcal{D}^{\mathcal{MP}}$, respectively.

Type 2: Stand-By Mode. If the Kinect was not streaming any data (OpenNI XnSensorServer is shut down) but connected to USB and power, it stayed in a stand-by mode (green LED was still flashing). Regarding an application using the Kinect, this is the typical mode between the application's termination and the next access to the Kinect. After warm-up, the stand-by mode was entered for 15 minutes before returning to the on-line mode. The changes in $\mathcal{D}^{\mathcal{D}}$ and $\mathcal{D}^{\mathcal{MP}}$ were -3.09 and 0.73 mm. To determine maximal changes, the stand-by mode was entered for 10 hours. We determined -5.95 and 1.67 mm regarding $\mathcal{D}^{\mathcal{D}}$ and $\mathcal{D}^{\mathcal{MP}}$. This corresponds to approx. 25% of the changes compared to the power-on and the fan cooling scenario (cf. Sec. 4.1 and 4.3). This smaller change is due to Kinect's power consumption, that was comparable in the stand-by and the on-line mode. This prevented a cooling of Kinect's internal components. Thus the last rule is: *Try to keep the Kinect always in the on-line mode. If this is not possible, leaving it in the stand-by mode is the best alternative.*

5 Conclusion

The analysis of several combinations of environmental and thermal conditions (stable and varying temperature, air draft, usage of fans, power disconnection etc.) has shown that they have a strong impact on the Kinect's output. Based on the findings temperature-related rules have been established which may help to reduce errors in the calibration and measurement process of the Kinect. Future work will include finding a model which describes the depth error in relation to the temperature, and developing a correction function based on this model.

References

1. Smisek J., Jancosek M., Pajdla T.: 3D with Kinect. International Conference on Computer Vision Workshops (ICCV Workshops, IEEE), p.1154-1160 (2011)
2. Stowers J., Hayes M., Bainbridge-Smith A.: Quadrotor Helicopter Flight Control Using Hough Transform and Depth Map from a Microsoft Kinect Sensor. Conference on Machine Vision Applications, MVA2011, Nara, Japan (2011)
3. Khoshelham K., Elberink S.O.: Accuracy and resolution of Kinect depth data for indoor mapping applications. Sensors: Journal on the science and technology of sensors and biosensors, pp. 1437-1454 (2012)
4. Berger K., Ruhl K., Brümmer C., Schröder Y., Scholz A., Magnor M.: Markerless Motion Capture using multiple Color-Depth Sensors. In Proc. Vision, Modeling and Visualization (VMV), pp. 317324 (2011)
5. Weinmann M., Wursthorn S., Jutzi B.: Semi-automatic image-based co-registration of range imaging data with different characteristics. PIA11 - Photogrammetric Image Analysis. ISPRS Archives 38(3)/W22, pp. 119-124 (2011)
6. Kahlmann T., Remondino F., Ingensand H.: Calibration for increased accuracy of the range imaging camera Swissranger. ISPRS Commission V Symposium Image Engineering and Vision Metrology, XXXVI, Part 5. Desden 25-27 (2006)
7. Bruhn A., Weickert J., Schnoerr C.: Lucas/Kanade meets Horn/Schunk: combining local and global optical flow methods. International Journal of Computer Vision (IJCV), 61(3):211231 (2005)
8. Baker S., Scharstein D., Lewis J.P., Roth S., Black M.J., Szeliski R.: A Database and Evaluation Methodology for Optical Flow. In Proc. Eleventh IEEE International Conference on Computer Vision (ICCV 2007), Rio de Janeiro, Brazil (2007)
9. Hartley R., Zisserman A.: Multiple View Geometry in Computer Vision. Second Edition, Cambridge University Press, New York, USA (2003)
10. Zhang Z.: A Flexible New Technique for Camera Calibration. Technical Report, MSR-TR-98-7, Microsoft Research Microsoft Corporation, One Microsoft Way, Redmond, WA 98052 (1998)
11. Bouguet J.Y.: Camera Calibration Toolbox for Matlab, `http://www.vision.caltech.edu/bouguetj/calib\_doc/index.html`
12. Microsoft Corporation, Kinect for Xbox 360, `http://www.xbox.com/de-DE/Kinect`
13. OpenNI - Open Natural Interaction, `http://openni.org/`
14. Hothmer J.: Possibilities and limitations for elimination of distortion in aerial photographs. Photogrammetric Record. 2(12): 426-445 (1958)
15. Smith M.J., Cope E.: The effect of temperature variation on single-lens-reflex digital camera calibration parameters. International Archives of Photogrammetry, Remote Sensing and Spatial Information Sciences, Vol. 28 (2010)